FULL PAPER

Nanostructure and Optoelectronic Characterization of Small Molecule Bulk Heterojunction Solar Cells by Photoconductive Atomic Force Microscopy

By *Xuan-Dung Dang, Arnold B. Tamayo, Junghwa Seo, Corey V. Hoven, Bright Walker,* and *Thuc-Quyen Nguyen**

Photoconductive atomic force microscopy is employed to study the nanoscale morphology and optoelectronic properties of bulk heterojunction solar cells based on small molecules containing a benzofuran substituted diketopyrrolopyrrole (DPP) core (3,6-bis(5-(benzofuran-2-yl)thiophen-2-yl)-2,5-bis(2-ethylhexyl)pyrrolo[3,4-c]pyrrole-1,4-dione, DPP(TBFu)$_2$, and [6,6]–phenyl-C$_{71}$-butyric acid methyl ester (PC$_{71}$BM), which were recently reported to have power conversion efficiencies of 4.4%. Electron and hole collection networks are visualized for blends with different donor:acceptor ratios. Formation of nanostructures in the blends leads to a higher interfacial area for charge dissociation, while maintaining bicontinuous collection networks; conditions that lead to the high efficiency observed in the devices. An excellent agreement between nanoscale and bulk open-circuit voltage measurements is achieved by surface modification of the indium tin oxide (ITO) substrate by using aminopropyltrimethoxysilane. The local open-circuit voltage is linearly dependent on the cathode work function. These results demonstrate that photoconductive atomic force microscopy coupled with surface modification of ITO substrate can be used to study nanoscale optoelectronic phenomena of organic solar cells.

1. Introduction

Organic solar cells have obtained much attention in both academia and industry because of their potential to produce low-cost plastic devices for alternative energy sources.[1,2] In these devices, light absorbed by the donor and the acceptor materials creates excitons, which have binding energies of about 0.4 eV[3,4] and diffusion lengths of about 10 nm.[5,6] Bulk heterojunction (BHJ) architectures comprising mixtures of electron donor and acceptor components with aligned frontier orbitals have been utilized to efficiently dissociate excitons and collect the charge carriers.[7,8] The external quantum efficiency depends on the incident light absorption, the exciton dissociation efficiency/charge generation, charge transport, and the carrier collection efficiency.[9–11] Film processing conditions such as choice of solvent, additives, solvent vapor and thermal annealing have been used to control the film morphology and optimize the donor/acceptor interfacial area for exciton dissociation, while retaining the bicontinuous networks needed for efficient charge transport and collection.[12–14] Hence, there has been substantial effort to understand how morphological modifications affect the composite set of phenomena that determine the overall device performance.[15,16]

Atomic force microscopy, a form of scanning probe microscopy, is a common technique used to examine the surface morphology of organic thin films. Other forms of scanning probe microscopy can enable simultaneous local probing of surface morphology, electrical properties, and optical properties.[15,17–21] For instance, scanning Kelvin probe microscopy has been used to study the photoinduced charge generation in polyfluorene-based photovoltaic structures, revealing a correlation between surface photovoltage and blend morphology.[19] Time-resolved electrostatic force microscopy has been applied to study the dynamics of photogenerated carriers in polymer-polymer blends.[21] In these two scanning probe techniques, the conductive probe is not in contact with the surface. Although valuable information on photoinduced charge generation in BHJ films can be extracted, these techniques do not provide information on charge transport and collection properties. Recently, conductive atomic force microscopy (C-AFM) has been shown to be a useful tool for characterization of nanoscale phase separation and charge transport in blends containing poly(3-hexylthiophene) and [6,6]-phenyl C61-butyric acid methyl ester (P3HT:PCBM).[22–24] In this mode, a conductive probe contacts the sample surface (the tip acts as a nanoelectrode) to measure current as a function of applied voltage at a specific point on the surface (local

[*] Dr. X.-D. Dang, Dr. A. B. Tamayo,[†] Dr. J. H. Seo, C. V. Hoven, B. Walker, Prof. T.-Q. Nguyen
Departments of Chemistry & Biochemistry
Department of Materials
Institute for Polymers and Organic Solids
University of California
Santa Barbara, CA 93106 (USA)
E-mail: quyen@chem.ucsb.edu

[†] Present address: Department of Chemistry and Geochemistry, Colorado School of Mines, Golden, CO 80401 (USA)

ADVANCED
FUNCTIONAL
MATERIALS
www.afm-journal.de

Materials
Views
www.MaterialsViews.com

current–voltage, I–V, curve) or to map out the current image at a fixed bias. The nanoscale charge mobility can be extracted from the I–V characteristics. By selecting the work function of the metal-coated probe, one can select the type of carriers injected into the sample. This technique provides information about charge transport networks but does not provide information on photoinduced charge generation processes. Recently, Ginger and coworkers demonstrated that the photocurrent obtained by using the photoconductive AFM (pc-AFM) technique, i.e. a C-AFM equipped with a laser as a light source, correlates well with bulk device performance.[15,16,25] Thus, pc-AFM provides a powerful technique for nanoscale characterization of organic solar cells since it can provide not only a comprehensive picture of nanoscale phase separation, surface morphology and photoinduced charge generation at the film surface, but also information on the surface charge collection networks.

In this work, we use pc-AFM to elucidate the nanoscale morphological and optoelectronic properties of BHJ films containing 3,6-bis(5-(benzofuran-2-yl)thiophen-2-yl)-2,5-bis(2-ethylhexyl) pyrrolo[3,4-c]pyrrole-1,4-dione (DPP(TBFu)$_2$) as the donor and [6,6]–phenyl-C$_{71}$-butyric acid methyl ester (PC$_{71}$BM) as the acceptor. Solar cells prepared from DPP(TBFu)$_2$ and PC$_{71}$BM cast from chloroform solution were recently reported to have a power conversion efficiencies (η) of 4.4%,[26] which is comparable to the efficiency of BHJ polymer-based solar cells.[27,28] The performance of DPP(TBFu)$_2$ is better than other closely related structural analogs thus it is important to understand the nanoscale properties and the origin of the high performance. We apply pc-AFM to probe electron- and hole- collection networks with a resolution of ~20 nm and correlate the surface morphology with local photocurrent generation and open-circuit voltage. We also studied the influence of donor:acceptor ratio on the film morphology and photocurrent. Differences between nanoscale and bulk device performance are discussed. Furthermore, by modifying the work function of the substrate, a direct correlation between nanoscale open-circuit voltage (V_{oc}) and the electrode work function is observed.

2. Results and Discussion

In dark and pc-AFM measurements, a bias was always applied to the substrate. Due to the high work function of the gold-coated probe (ϕ_{Au} ~ 5.10 eV) and the lower work function of the indium tin oxide (ITO) (ϕ_{ITO} ~ 4.76 eV), the direction of current flow is the opposite of conventional bulk solar cells with ITO/ poly(3,4-ethylenedioxythiophene):poly(styrenesulfonate) (PEDOT:PSS) anode and aluminum cathode (ϕ_{Al} ~ 4.30 eV). The work function of the PEDOT:PSS used in this study is approximately 4.90 eV as determined by ultraviolet photoelectron spectroscopy. Two data collection modes are used: a conductive probe contacts

the sample surface to measure current as a function of applied voltage at a specific point on the surface (local I–V curve) or to map out the current image at a fixed bias. These two types of measurements can be done in the dark or under illumination. For our measurements, V_{oc} is defined as a bias at which the photocurrent is zero and is extracted from the nanoscale photocurrent-voltage curve.

To maximize the power conversion efficiency of BHJ solar cells, the choice of donor and acceptor composition must be considered since it impacts the absorption, morphology and charge transport.[5,23,29,30] Here, we investigated the effect of donor:acceptor ratio on the nanoscale phase separation and photogeneration of DPP(TBFu)$_2$:PC$_{71}$BM films on the ITO/PEDOT substrates annealed at 100 °C for 10 min. **Figure 1** shows 2 µm × 2 µm surface topography and photocurrent images of annealed DPP(TBFu)$_2$:PC$_{71}$BM films prepared at 70:30, 50:50, and 30:70 ratios. One notes that the root mean square (RMS) surface roughness remains relatively constant with the acceptor content, 1.1 nm, 1.4 nm, and 1.5 nm for 70:30, 50:50, and 30:70 blends, respectively. However, the surface morphology changes substantially as a function of component ratio. For 70:30 and 50:50 ratios, the films comprise connected fiber-like structures. Greater PC$_{71}$BM content in the films leads to isolated donor-rich domains on the surface, and hence, a slightly higher RMS value (Figure 1c). However, the donor-rich domains are distributed homogeneously.
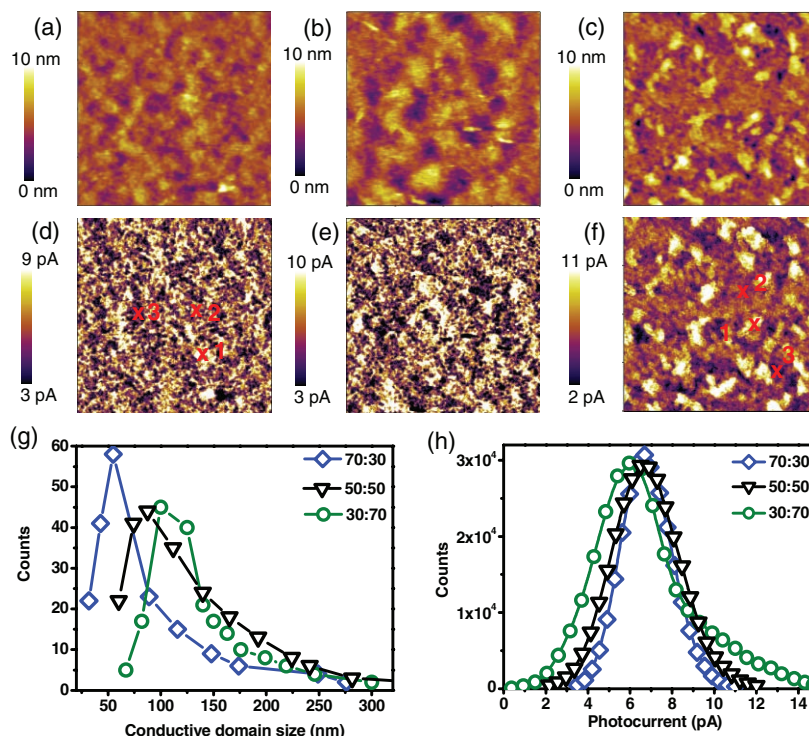

Figure 1. Topography (a–c) and photocurrent images of 70:30 (left), 50:50 (middle) and 30:70 (right) DPP(TBFu)$_2$:PC$_{71}$BM films collected at 0 V (d–f). All samples were annealed at 100 °C for 10 min under nitrogen. Conductive domain size distribution (g) and nanoscale photocurrent histogram (h) of different DPP(TBFu)$_2$:PC$_{71}$BM ratios analyzed from (d), (e) and (f). Marked locations in (d) and (f) were used for recording nanoscale photocurrent-voltage characteristics presented in Figure 4a and light intensity dependence of short-circuit photocurrent as shown in Figure 5a. Image sizes are 2 µm × 2 µm.

Materials
Views
www.MaterialsViews.com

ADVANCED
FUNCTIONAL
MATERIALS
www.afm-journal.de

FULL PAPER

To further confirm that the isolated domains are donor rich, dark current images were collected using gold-coated probes. Due to the high work function of the gold-coated probe, only holes are injected into the film and transported through the donor networks at –1 V.[23] One observes that the isolated domains in the 30:70 film have a higher injected hole current than their surroundings (Figure S1, Supporting Information).

Figure 1d–f show the photocurrent images for the three blend ratios collected at 0 V (short-circuit photocurrent condition) using gold-coated silicon probes. For the 70:30 and 50:50 blended films, connected fibrous structures with a diameter of 50–70 nm can be observed in the photocurrent images and the conductive domain size distribution (Figure 1g). No micrometer size phase separation is observed. For the 30:70 blend, the conductive fibrous structures increases to ~110 nm in diameter (Figure 1g), and the high photocurrent domains correspond to the isolated domains observed in the topography image (Figure 1c). Lower donor content leads to larger variation in photocurrent levels (green curve, Figure 1h). One surmises that the larger conductive domains result in a smaller donor:acceptor interfacial area for charge separation, and hence, a lower device efficiency, consistent with the observation that the power conversion efficiency of annealed bulk devices decreases from 4.2% to 2.0% when the donor:acceptor ratio changes from 70:30 to 30:70.[26]

To image donor and acceptor networks, we collected current images under illumination as a function of bias polarization. We consider first the 30:70 films with a large phase separation (Figure 1c,f) wherein the tall features are indentified as a key for monitoring the carrier flow direction with bias polarity. **Figure 2**

shows the nanoscale photocurrent images collected at positive biases (a,b), 0 V (c), and negative biases (d–g) and dark current image collected at –1.5 V (h). Due to the high work function of the gold-coated probes, holes are collected by the AFM probe and the electrons are collected by the ITO/PEDOT:PSS electrode at applied biases greater than the V_{oc} (–0.22 V) as evidenced by positive photocurrent at short-circuit condition in Figure 1d–f and Figure 2a–c. A similar result is also observed for an active layer deposited directly atop an ITO substrate. This charge collection process is similar to what observed in an inverted solar cell structure.[31,32] It should be noted that this nanoscale result is different from bulk devices with *evaporated* Au electrodes atop the active layer, where a dipole at the Au interface significantly affects the work function of the electrode and the V_{oc}.[33,34] As holes are being collected by the tip in Figure 1d–f and Figure 2c,d, the regions with high current in the photocurrent images should correspond to donor-rich domains. Photocurrent collected at a bias close to V_{oc} is negligible. When a small negative bias, e.g., –0.5 V, beyond the V_{oc} of –0.22 V is applied to the substrate; the electric field in the device is reversed and the photogenerated holes travel toward the ITO/PEDOT:PSS electrode while the AFM probe collects the electrons. Therefore, the high and low current domains in Figure 2e (V = –0.5 V) are reversed to what is observed in Figure 2a,b because here the high current regions correspond to the acceptor-rich domains at the surface. The dark current collected at –0.5 V is negligible.

At a large enough negative bias hole injection from the tip dominates the current image collected at V = –1.5 V under illumination as shown in Figure 2g. At such a condition, the donor-rich domains show higher current than the surrounding similar to what observed in Figure 2a–c. The dark current image collected at the same bias (Figure 2h) shows much lower current level than that of the illuminated current, so the current observed at –1.5 V under illumination may be a combination of injected current and photoconductive gain[35–37] Thus, high current regions in current images collected at a small bias (–0.5 V) under illumination reveal acceptor networks whereas high current regions collected at small biases greater than the V_{oc} correspond to the donor-rich domains.

We now examine the electron and hole collection networks of the other two blends. Similar to the photocurrent images collected at 0 V, no large scale phase separation is observed for the 70:30 and 50:50 blends at positive and negative biases as shown in **Figure 3**. The increase in hole photocurrent level at +0.5 V, as compared to those current images collected at 0 V, is due to more efficient charge extraction at high electric field. At –0.5 V, the image collected from 70:30 comprises some isolated low current domains (Figure 3c); however, the number of low current regions decreases with increasing the acceptor content. The development of large phase-separated morphology with increasing PC$_{71}$BM results in
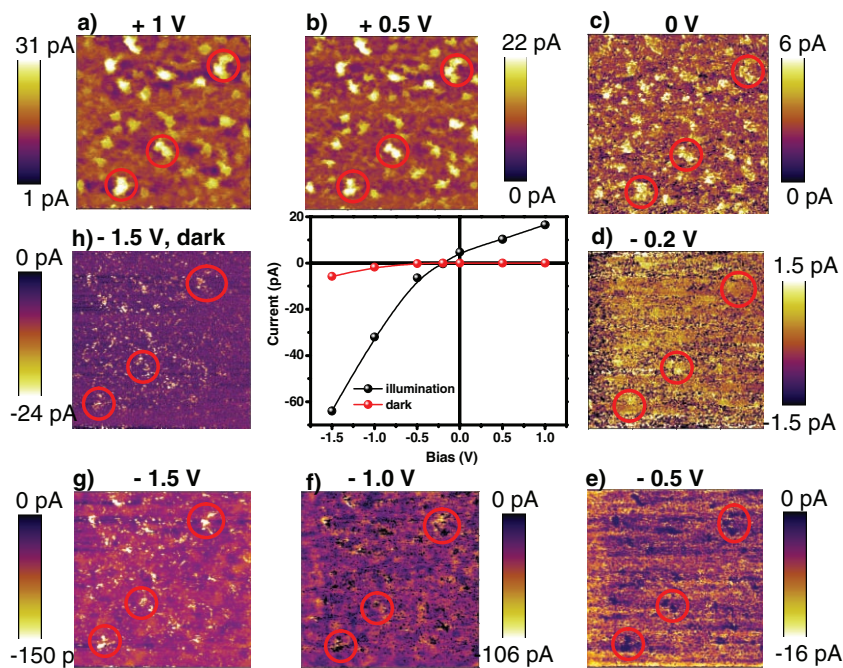

Figure 2. Photocurrent images of annealed 30:70 films collected at different biases at the same location: +1.0 V (a), +0.5 V (b), 0 V (c), –0.2 V (d), –0.5 V (e), –1 V (f), –1.5 V (g). Dark photocurrent image collected from the same location at –1.5 V is shown in (h). The scan sizes are 2 μm × 2 μm. Red circles highlight an evolution of current flow as a function of applied bias. Dark (red) and illuminated (black) I–V curves are constructed from the integrated current images corresponding to the applied biases.
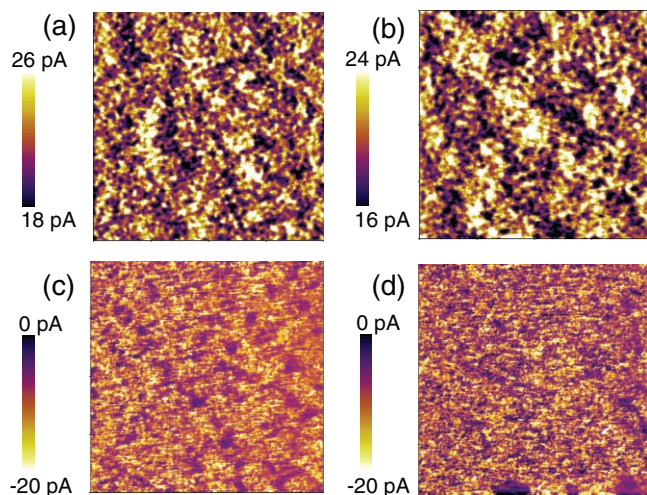
**ADVANCED
FUNCTIONAL
MATERIALS**

www.afm-journal.de

Materials Views

www.MaterialsViews.com

Figure 3. Photocurrent images of annealed 70:30 (left), 50:50 (right) $DPP(TBFu)_2$:$PC_{71}BM$ films collected at +0.5 V (a, b), and at −0.5 V (c, d) at the same locations with the topographical images shown in Figure 1. Image sizes are 2 μm × 2 μm.

fewer interfaces for charge dissociation, and perhaps, to a less continuous network to transport charges. These results can explain why the short-circuit current and efficiency are lower in the 30:70 bulk device (5.7 mA cm^{-2}, 2%) than in 70:30 and 50:50 devices (9.0 mA cm^{-2}, 4.2% and 8.4 mA cm^{-2}, 3.4% respectively).[26]

Figure 4a shows the nanoscale photocurrent versus bias of annealed 30:70 $DPP(TBFu)_2$:$PC_{71}BM$ film collected at different locations. The locations are marked in the topography image shown in Figure 1f. We collected nanoscale photocurrent versus bias at different locations (Figure S2, Support Information); however, only three representative curves are shown in Figure 4a. There is a strong spatial variation in the V_{oc} and short-circuit current (I_{sc}). Higher I_{sc} is found in regions with high photocurrent corresponding to donor rich domains. It appears that the discrepancy in the I_{sc} is related to changes in local environment due to different molecular packing[38] and/or local composition and ordered nanostructure within the domains[21–23] and/or surface accumulation of the different components.[39] Average I–V characteristics of the annealed 30:70, 50:50, and 70:30 $DPP(TBFu)_2$:$PC_{71}BM$ films are shown in Figure 4b. The average nanoscale I_{sc} of the annealed 30:70, 50:50 and 70:30 $DPP(TBFu)_2$:$PC_{71}BM$ films are 4.3 ± 4.9 pA, 7.8 ± 6.7 pA, and 9.6 ± 6.0 pA, respectively. The high I_{sc} value for the 70:30 $DPP(TBFu)_2$:$PC_{71}BM$ films can be explained by the formation of nanoscale phase separation and continuous networks, providing more suitable donor:acceptor interfaces and resulting in efficient exciton dissociation and charge collection. Adding more $PC_{71}BM$ to the blends generates a larger phase separation which can reduce the interfaces and interrupt charge collection pathways.

Figure 4a also shows a large variation in the V_{oc} from one location to another. The V_{oc} collected at location 1 is ∼−0.05 V, much smaller than those collected from locations 2 and 3 (−0.12 V and −0.27 V, respectively). The V_{oc} variation was previously attributed to differences in local environment and/or
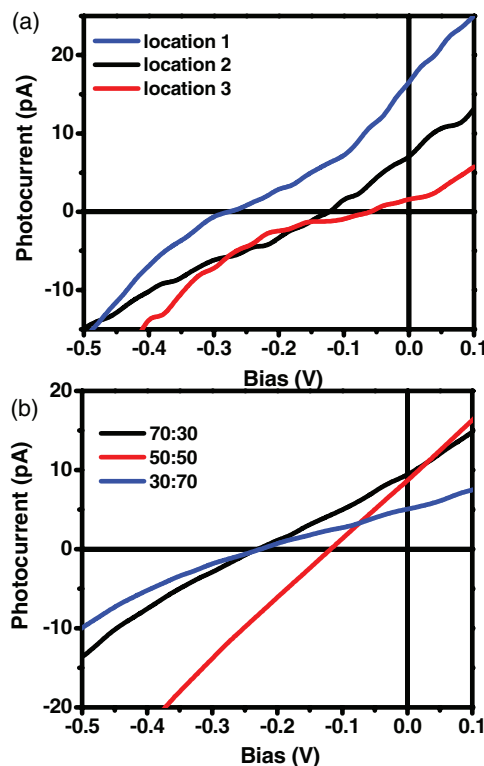

Figure 4. a) Nanoscale photocurrent versus bias of 30:70 $DPP(TBFu)_2$:$PC_{71}BM$ film collected at different locations marked in Figure 1f and b) average nanoscale photocurrent versus bias of different $DPP(TBFu)_2$:$PC_{71}BM$ ratios.

variation in the local work function and conductivity of the ITO/PEDOT:PSS.[15,40] The average nanoscale V_{oc} are −0.22 ± 0.1 V, −0.12 ± 0.1 V, and −0.22 ± 0.1 V for the 70:30, 50:50, and 30:70 films, respectively. The V_{oc} is slightly higher in the films comprising high donor content. Nanoscale V_{oc} values are much smaller than that of actual devices that use Al electrodes, which is 0.9 V.[26] The result also implies that the nanoscale V_{oc} does not depend on just the energy level difference between the donor highest occupied molecular orbital (HOMO) and the acceptor lowest unoccupied molecular orbital (LUMO). The smaller V_{oc} derived from nanoscale measurement is a result of using a high work function of gold tip[41] in an inverted device structure. Small V_{oc} values obtained in nanoscale measurement (0.05 V) compared to the bulk device (0.65 V) has also been observed for P3HT:PCBM with a similar configuration of pc-AFM measurements.[25]

Next, we investigate the light intensity dependence of the nanoscale I_{sc} (**Figure 5**). In the bulk devices, I_{sc} increases with the incident light intensity (P), according to a power-law behavior $I_{sc} \propto P^{\alpha}$. The power-law component α is suggestive of the degree of photogenerated free carrier loss and is dependent on parameters such as unbalanced electron/hole mobilites and nanoscale morphology.[42–45] When α is unity, all photogenerated free carriers are collected. The α is less than unity, indicating recombination[45] or space charge limited photocurrent.[44] At high illumination intensities, the intensity dependence
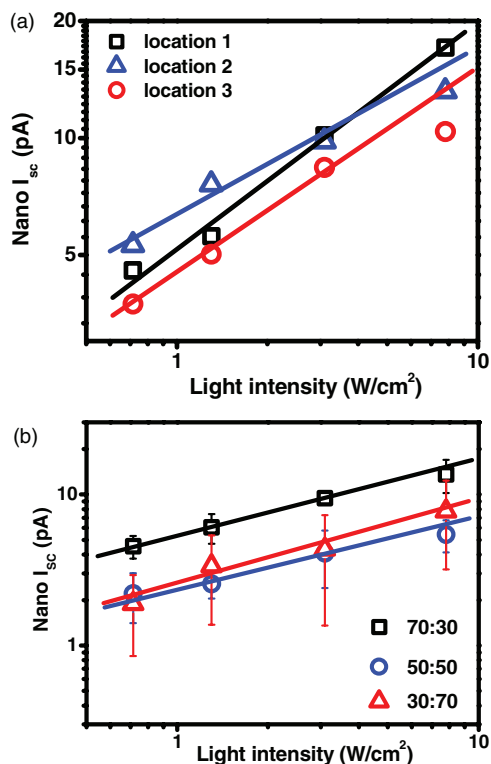
Figure 5. a) Light intensity dependence of the nanoscale I_{sc} collected at different locations marked in Figure 1d for 70:30 DPP(TBFu)$_2$:PC$_{71}$BM film and b) the average nanoscale I_{sc} value versus light intensity of different DPP(TBFu)$_2$:PC$_{71}$BM ratios collected using gold-coated silicon probe. The solid lines are the best fit through data points.

Figure 6. Topography (a,b) and photocurrent (c,d) images of annealed APTMS-ITO/55:45 P3HT:PC$_{71}$BM (left) and annealed APTMS-ITO/70:30 DPP(TBFu)$_2$:PC$_{71}$BM (right) collected at 0 V using gold-coated silicon tip. Photocurrent–voltage curves were collected at different locations marked in (b and d), but for P3HT:PC$_{71}$BM device the I–V curve is averaged from 20 different locations. Image sizes are 5 μm × 5 μm.

of I_{sc} becomes sublinear, similar to bulk measurements.[44] As in the case of nanoscale photocurrent-voltage characteristics (Figure 5a), the light intensity dependence of the I_{sc} varies from location to location, suggesting strong spatial variations in the device performance. The α value varies from 0.58 for location 1, to 0.43 for location 2, and to 0.53 for location 3. The dependence of the nanoscale I_{sc} on the light intensity in different blends is also shown in Figure 5b. Each data point in Figure 5b is an average of 50 I–V curves. Some of the I–V curves collected at different light intensity is included in Figure S3 of the Supporting Information. The α values are 0.50 ± 0.01, 0.45 ± 0.04, and 0.55 ± 0.05 for the 70:30, 50:50, and 30:70 DPP(TBFu)$_2$:PC$_{71}$BM ratios, respectively. This observation is in agreement with the low fill factor of bulk devices previously described.[26] However, the origin of such dependence remains unclear at this point.

A method was sought to improve the V_{oc} in nanoscale devices. To do so, we modified the work function of ITO and eliminated the PEDOT:PSS layer such that ITO would act as the cathode similar to Al cathode in the actual devices. We found that an aminopropyltrimethoxysilane (APTMS)-modified ITO substrate reduces the work function of the ITO from 4.75 eV to 4.30 eV similar to that of Al. The surface topographic images of different ITO substrates are included in Figure S4 of the Supporting Information. To prove that this method works, we first tested an annealed P3HT:PC$_{71}$BM active layer. **Figure 6**
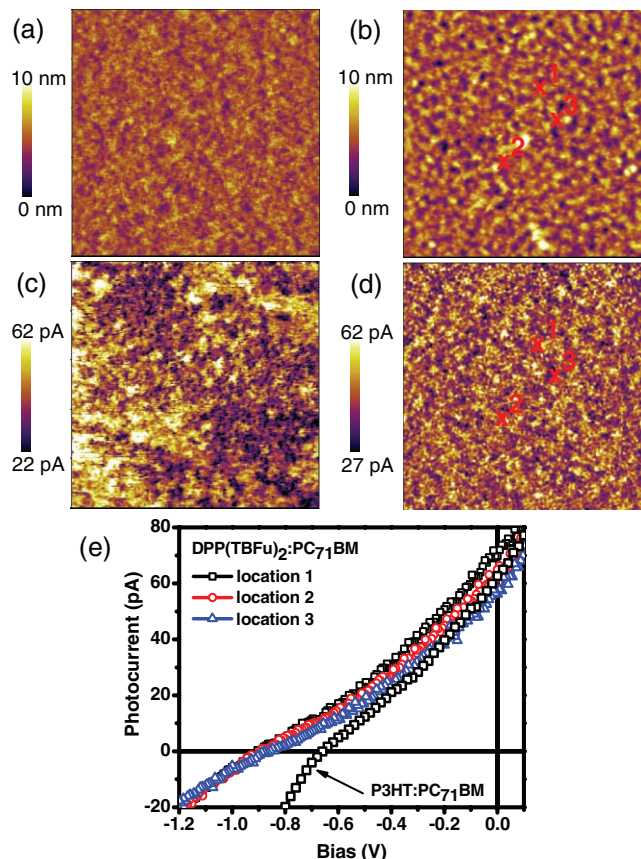
shows the topography and zero-bias photocurrent images of APTMS-ITO/55:45 P3HT:PC$_{71}$BM/Au tip and APTMS-ITO/70:30 DPP(TBFu)$_2$:PC$_{71}$BM/Au tip. The topographic image of annealed P3HT:PC$_{71}$BM films (Figure 6a) is similar to that observed previously;[25] however, the photocurrent, I_{sc}, and V_{oc} are enhanced significantly, as seen in Figure 6c and 6e. Figure 6b and 6d show the topographic and photocurrent images of annealed DPP(TBFu)$_2$:PC$_{71}$BM collected at the same light intensity and contact force to those images shown in Figure 1a and 1d. There is no significant difference in the surface topography between the films spun cast on ITO/PEDOT:PSS and APTMS-ITO substrates. The surface roughness increases slightly to ~1.4 nm, compared with ~1.0 nm for the films deposited on top of ITO/PEDOT:PSS substrates, but the photocurrent level is almost three times higher, indicating that the charge collection is more efficient for APTMS-ITO/DPP(TBFu)$_2$:PC$_{71}$BM.

Figure 6e shows the nanoscale photocurrent-voltage curves for annealed P3HT:PC$_{71}$BM and DPP(TBFu)$_2$:PC$_{71}$BM. One observes that the nanoscale device performance is improved significantly as compared to the devices deposited on ITO/PEDOT:PSS substrates. The nanoscale V_{oc} of P3HT:PC$_{71}$BM

FULL PAPER

is -0.65 ± 0.05 V similar to the value obtained from the actual devices,[4] indicating that the approach of using modifying ITO surface is valid. Nanoscale V_{oc} values collected from different regions of the 70:30 DPP(TBFu)$_2$:PC$_{71}$BM film are -0.88 ± 0.05 V, similar to the value obtained from the bulk device.[26] In this case, the V_{oc} is correlated well to the difference between the acceptor LUMO and the donor HOMO levels.[43,46] The nanoscale I_{sc} is much higher than that collected from the blend atop the ITO/PEDOT:PSS substrates. The short circuit current is 60 ± 12 pA, almost five times higher than that of ITO/PEDOT:PSS substrate (Figure 4a).

For bulk devices, the origin of the V_{oc} is complex and remains under debate. For instance, the V_{oc} is believed to depend on the difference between the donor HOMO and the acceptor LUMO;[43,47] however, changes in the V_{oc} value due to the electrode work function have been reported by several groups.[43,46,48,49] Thus, we examined the nanoscale V_{oc} values as a function of the electrode work function. **Figure 7a** shows the nanoscale $I-V$ characteristics of 70:30 DPP(TBFu)$_2$:PC$_{71}$BM films deposited on different modified ITO substrates: clean ITO, activated ITO (hydroxylated ITO surface), ITO/PEDOT:PSS, and APTMS-modified ITO. Each $I-V$ curve in Figure 7a is averaged from 20 different locations (Figure S5, S6, and S7, Supporting Information), indicating greatly improved device characteris-

tics compared to the devices on ITO/PEDOT:PSS substrates. The I_{sc} is 12 ± 4 pA for ITO/PEDOT:PSS, 16 ± 7 pA for films on cleaned ITO, 25 ± 5 pA for activated ITO, and 60 ± 12 pA for APTMS-modified ITO. As expected, the V_{oc} decreases with increasing the ITO work function. Figure 7b plots the V_{oc} as a function of the work function of various ITO substrates. ITO/PEDOT:PSS has a work function of 4.85 ± 0.5 eV.[50] A linear relationship between the V_{oc} and the work function is observed, which can be explained by changes in built-in potential due to the work function difference between anode and cathode electrodes.[49–51] This result has the important implication that by selecting suitable electrode materials, the V_{oc} can be maximized and accordingly leading to enhanced charge extraction and improved device performance.

It is important to note that there are several differences between the nanoscale and bulk device measurements. For the bulk devices, the Al top electrode is thermally evaporated on the active layer and is used for electron collection whereas in pc-AFM measurements, the gold or platinum coated tip is in physical contact with the film and is used to collect holes; therefore, the nature of the top electrode contact and its function are different. Ideally, one would like to use Al-coated tips; however, Al-coated tips degrade quickly. The difference in the device configuration is expected to have different charge collection efficiencies. Additionally, the light intensity is quite different between pc-AFM measurements (7.8 W cm^{-2}) and bulk device measurements (100 mW cm^{-2}). It is well documented that I_{sc} increases with increasing light intensity.[51,52] Finally, the high field concentrated in the AFM tip may lead to more efficient charge collection.[15,22,25] Despite the differences between the nanoscale and bulk measurements, important information can be obtained from the nanoscale study such as film morphology, photocurrent generation, photocurrent distribution on surface, conductive domain size distribution, mapping the donor and acceptor networks, and variation of V_{oc} and I_{sc} from location to location. For our system, the nanoscale results correlate well to the bulk measurement, and the surface topography and photocurrent imaging can help to explain why annealed bulk devices based on DPP(TBFu)$_2$:PC$_{71}$BM system are very efficient, relative to other molecular donor systems.[25]
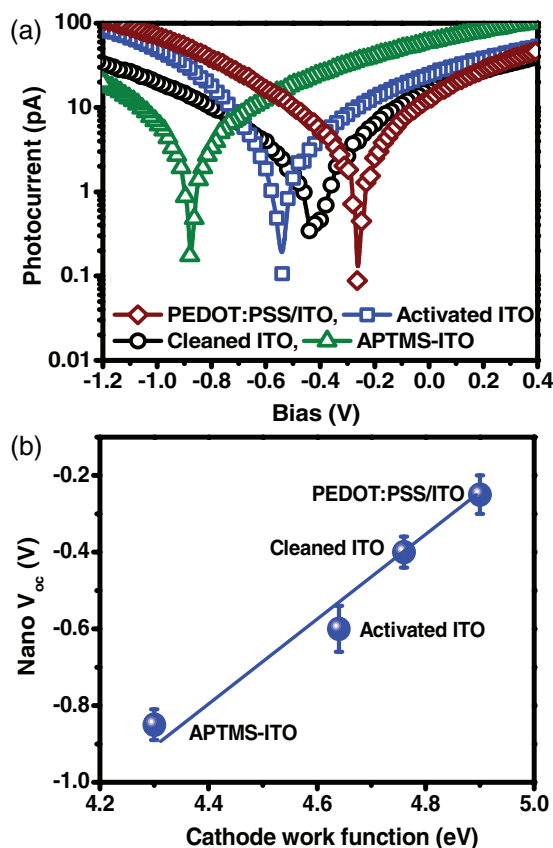

3. Conclusion

We have demonstrated the use of pc-AFM for nanoscale characterization of small molecule solution processed BHJ solar cells. Applying a small positive or negative bias to collect photocurrent images allows one to observe hole and electron collection networks, respectively. The phase separation depends strongly on the donor:acceptor ratio as observed in the topography and photocurrent images, which in turn, influences the charge generation and collection and the nanoscale solar cell efficiency. We found that large phase separation in the 30:70 blend results in lower short circuit current. The well-defined nanostructures of DPP(TBFu)$_2$:PC$_{71}$BM films explain the high efficiency of BHJ solar cells ($\eta \sim 4.4\%$) based on this small molecule system.[26] We have also developed a method to modify the ITO work function for nanoscale characterization of solar cell materials. The results reveal

Figure 7. a) Nanoscale $I-V$ characteristics of 70:30 DPP(TBFu)$_2$:PC$_{71}$BM deposited atop different cathodes and b) nanoscale V_{oc} versus work function of cathode electrode.

www.MaterialsViews.com

ADVANCED
FUNCTIONAL
MATERIALS
www.afm-journal.de

FULL PAPER

that at the nanoscale the active layer deposited atop APTMS-modified ITO has higher nanoscale photocurrent than using ITO/PEDOT:PSS substrates and similar V_{oc} to the actual devices. More interestingly, the local V_{oc} is linearly dependent on the substrate work function. Overall, results described here demonstrate that pc-AFM is a powerful technique to characterize solar cell materials and can be used to understand the bulk performance.

4. Experimental Section

Device fabrication involves spin coating a 45 nm PEDOT:PSS layer (Baytron P VP Al 4083) on cleaned ITO substrates (Thin Film Devices, Inc.). The film was then heated at 140 °C for 15 min before spin casting a 85 nm layer of DPP(TBFu)$_2$:PC$_{71}$BM from chloroform at different ratios at a speed of 2500 rpm for 30 s. The resulting samples were annealed at 100 °C for 10 min in a nitrogen glove box. For nanoscale device structures, aminopropyltrimethoxysilane (APTMS)-modified ITO substrates with work functions of 4.76 eV, 4.64 eV, and 4.30 eV, respectively, were used.[53] To activated the ITO surface, cleaned ITO substrates were soaked in H$_2$O:NH$_3$:H$_2$O$_2$ (5:1:1 by volume) solution for 15 min to form hydroxylated surface.[54,55] Next, the activated ITO substrates were soaked in a 1% APTMS in methanol. This procedure results in a self-assembled monolayer of APTMS atop of ITO,[53] producing substrates with a work function of 4.30 eV, which is similar to that of aluminum. For thermal annealing, the 70:30 blends were spun cast on the substrates and then baked at 100 °C for 10 min in the glove box. For a comparative study, 55:45 P3HT:PC$_{71}$BM films were spun cast on the APTMS-ITO substrates from the 1.8% (w/v) solution in chlorobenzene at 2000 rpm for 40 s. The final films were then annealed at 150 °C for 15 min in the glove box. pc-AFM measurements were performed with an Asylum Research MFP-3D microscope sitting atop of an inverted optical microscopy (Olympus, IX71). All measurements were done using a nitrogen flow cell. In this work, the bias was applied to the substrate, and the current was recorded by internal preamplifier (Asylum Research ORCA head model). Gold-coated silicon probes with a spring constant of 0.2 nN m^{-1} and resonant frequency of 13 kHz (Budget Sensors) were used. A green light source (X-Cite series 120PC Q) with a wavelength of 532 nm and a power of 7.8 W cm^{-2} was used for photocurrent imaging and local I–V measurements, unless otherwise stated. The light was focused on the sample through an inverted optical microscope (Olympus) and then the tip was positioned at the center of the illumination spot. The illuminated spot size at the sample surface was measured to be approximately 160 μm in diameter.

Supporting Information

Supporting Information is available online from Wiley InterScience or from the author.

Acknowledgements

[1] J. Nelson, *Science* **2001**, *293*, 1059.

[2] F. C. Krebs, *Sol. Energy Mater. Sol. Cells* **2009**, *93*, 394.

[3] M. D. McGehee, *Nat. Photonics* **2009**, *3*, 250.

[4] G. Dennler, M. C. Scharber, C. J. Brabec, *Adv. Mater.* **2009**, *21*, 1323.

[5] H. Hoppe, N. S. J. Sariciftci, *Mater. Chem.* **2006**, *16*, 45.

[6] X. N. Yang, J. Loos, S. C. Veenstr, W. H. Verhees, M. M. Wienk, J. M. Kroon, M. A. J. Michels, R. A. J. Janssen, *Nano Lett.* **2005**, *5*, 579.

[7] G. Yu, J. Gao, J. C. Hummelen, F. Wudl, A. J. Heeger, *Science* **1995**, *270*, 1789.

[8] J. J. M. Halls, C. A. Walsh, N. C. Greenham, E. A. Marseglia, R. H. Friend, S. C. Moratti, A. B. Homes, *Nature* **1995**, *376*, 498.

[9] P. Peumans, A. Yakimov, S. R. Forrest, *J. Appl. Physiology* **2003**, *93*, 3693.

[10] J. Peet, J. Y. Kim, N. E. Coates, W. L. Ma, D. Moses, A. J. Heeger, G. C. Bazan, *Nat. Mater.* **2007**, *6*, 479.

[11] S. Guenes, H. Neugebauer, N. S. Sariciftci, *Chem. Rev.* **2007**, *107*, 1324.

[12] J. Peet, A. J. Heeger, G. C. Bazan, *Acc. Chem. Res.* **2009**, *42*, 1700.

[13] M. C. Quiles, T. Ferenczi, T. Agostinelli, P. G. Etchegoin, Y. Kim, T. D. Anthopoulos, P. N. Stavrinou, D. D. C. Bradley, J. Nelson, *Nat. Mater.* **2008**, *7*, 158.

[14] J. Peet, M. L. Senatore, A. J. Heeger, G. C. Bazan, *Adv. Mater.* **2009**, *21*, 1521.

[15] D. C. Coffrey, O. G. Reid, D. B. Rodovsky, G. P. Bartholomew, D. S. Ginger, *Nano Lett.* **2007**, *7*, 738.

[16] T. A. Bull, L. S. C. Pingree, S. A. Jenekhe, D. S. Ginger, C. K. Luscombe, *ACS Nano* **2009**, *3*, 627.

[17] H. Hoppe, T. Glatzel, M. Niggemann, A. Hinsch, M. Ch. Lux-Steiner, N. S. Sariciftci, *Nano Lett.* **2005**, *5*, 269.

[18] H. J. Snaith, A. C. Arias, A. C. Morteani, C. Silva, R. H. Friend, *Nano Lett.* **2002**, *2*, 1353.

[19] M. Chiesa, L. Brgi, J.-S. Kim, R. Shikler, R. H. Friend, H. Sirringhaus, *Nano Lett.* **2005**, *5*, 559.

[20] A. Liscio, G. D. Luca, F. Nolde, V. Palermo, K. Millen, P. Samor, *J. Am. Chem. Soc.* **2008**, *130*, 780.

[21] D. C. Coffey, D. S. Ginger, *Nat. Mater.* **2006**, *5*, 735.

[22] O. G. Reid, K. Munechika, D. S. Ginger, *Nano Lett.* **2008**, *8*, **1602**.

[23] D. Mark, J. Peet, T.-Q. Nguyen, *J. Phys. Chem. C* **2008**, *112*, 7241.

[24] O. Douheret, L. Lutsen, A. Swinnen, M. Breselge, K. Vandewal, L. Goris, J. Manca, *Appl. Phys. Lett.* **2007**, *89*, 032107.

[25] L. S. C. Pingree, O. G. Reid, D. S. Ginger, *Nano Lett* **2009**, *9*, 2946.

[26] B. Walker, A. B. Tamayo, X.-D. Dang, P. Zalar, J. H. Seo, A. Garcia, M. Tantiwiwat, T.-Q. Nguyen, *Adv. Funct. Mater.* **2009**, *19*, 3063.

[27] W. Ma, C. Yang, X. Gong, K. Lee, A. J. Heeger, *Adv. Funct. Mater.* **2005**, *15*, 1617.

[28] M. Reyes-Reyes, K. Kim, D. L. Carroll, *Appl. Phys. Lett.* **2005**, *87*, 083506.

[29] A. B. Tamayo, X.-D. Dang, B. Walker, J. H. Seo, T. Kent, T.-Q. Nguyen, *Appl. Phys. Lett.* **2009**, *94*, 103301.

[30] C. Müller, T. A. M. Ferenczi, M. Campoy-Quiles, J. M. Frost, D. D. C. Bradley, P. Smith, N. Stingelin-Stutzmann, J. Nelson, *Adv. Mater.* **2008**, *20*, 3510.

[31] Z. Zu, L.-M. Chen, G. Yang, C. H. Huang, J. Hou, Y. Wu, G. Li, C. S. Hsu, Y. Yang, *Adv. Funct. Mater.* **2009**, *19*, 1227.

[32] S. K. Hau, H. L. Yip, H. Ma, A. K. Y. Jen, *Appl. Phys. Lett.* **93**, *23*, 233304.

[33] V. D. Mihailetchi, P. W. M. Blom, J. C. Hummelen, M. T. J. Rispens, *J. Appl. Phys.* **2003**, *94*, 6849.

[34] S. C. Veenstra, A. Heeres, G. Hadziioannou, G. A. Sawatzky, H. T. Jonkman, *Appl. Phys. A: Mater. Sci. Process.* **2002**, *75*, 661.

[35] H.-Y. Chen, M. K. F. Lo, G. Yang, H. G. Monbouquette, Y. Yang, *Nat. Nanotechnol.* **2008**, *3*, 543.

[36] I. H. Campbell, B. K. Crone, *J. Appl. Phys.* **2007**, *101*, 024502.

[37] M. Hiramoto, A. Miki, M. Yoshida, M. Yokoyama, *Appl. Phys. Lett.* **2002**, *81*, 1500.

FULL PAPER

[38] M. D. Perez, C. Borek, S. R. Forrest, M. E. Thompson, *J. Am. Chem. Soc.* **2009**, *131*, 9281.

[39] L. M. Chen, Z. Hong, G. Li, Y. Yang, *Adv. Mater.* **2009**, *21*, 1434.

[40] C. Ionescu-Zanetti, A. Mechler, S. A. Carter, R. Lal, *Adv. Mater.* **2004**, *16*, 385.

[41] C. J. Brabec, A. Cravino, D. Meissner, N. S. Sariciftci, T. Fromherz, M. T. Rispens, L. Sanchez, J. C. Hummelen, *Adv. Funct. Mater.* **2001**, *11*, 374.

[42] V. D. Mihailetchi, J. Wildeman, P. W. M. Blom, *Phys. Rev. Lett.* **2005**, *94*, 126602.

[43] L. J. A. Koster, V. D. Mihailetchi, P. W. M. Blom, *Appl. Phys. Lett.* **2005**, *87*, 203502.

[44] L. J. A. Koster, V. D. Mihailetchi, P. W. M. Blom, *Appl. Phys. Lett.* **2006**, *88*, 052104.

[45] M. Lenes, M. Morana, C. J. Brabec, P. W. M. Blom, *Adv. Funct. Mater.* **2009**, *19*, 1106.

[46] P. W. M. Blom, V. D. Mihailetchi, L. J. A. Koster, D. E. Markov, *Adv. Mater.* **2007**, *19*, 1551.

[47] M. C. Scharber, D. Mühlbacher, M. Koppe, P. Denk, C. Waldauf, A. J. Heeger, C. J. Brabec, *Adv. Mater.* **2006**, *18*, 789.

[48] V. D. Mihailetchi, P. W. M. Blom, J. C. Hummelen, M. T. J. Rispens, *J. Appl. Phys.* **2003**, *94*, 6849.

[49] H. J. Yip, S. K. Hau, N. S. Baek, H. Ma, A. K. Y. Jen, *Adv. Mater.* **2008**, *20*, 2376.

[50] K. Fehse, S. Olthof, K. Walzer, K. Leo, R. L. Johnson, H. Glowatzki, B. Broeker, N. Koch, *J. Appl. Phys. Lett.* **2007**, *102*, 073719.

[51] J. K. J. van Duren, X. Yang, J. Loos, C. W. T. Bulle-Lieuwma, A. B. Sieval, J. C. Hummelen, R. A. J. Janssen, *Adv. Funct. Mater.* **2004**, *14*, 425.

[52] I. Riedel, J. Parisi, V. Dyakonov, L. Lutsen, D. Vanderzande, J. C. Hummelen, *Adv. Funct. Mater.* **2004**, *14*, 38.

[53] K. Siskova, J. H. Seo, T.-Q. Nguyen, unpublished.

[54] R. Sfez, N. Peor, S. R. Cohen, H. Cohen, S. Yitzchaik, *J. Mater. Chem.* **2006**, *16*, 4044.

[55] R. Sfez, L. D.- Zhong, I. Turyan, D. Mandler, S. Yitzchaik, *Langmuir* **2001**, *17*, 2556.